Three-Dimensional Choroidal Vessels Assessment in Diabetic Retinopathy

Elham Sadeghi,[1] Katherine Du,[1] Oluwaseyi Ajayi,[1] Elli Davis,[2] Nicola Valsecchi,[1,3,4] Mohammed Nasar Ibrahim,[1] Sandeep Chandra Bollepalli,[1] Kiran Kumar Vupparaboina,[1] Jose Alain Sahel,[1] and Jay Chhablani[1]

[1]Department of Ophthalmology, University of Pittsburgh, School of Medicine, Pittsburgh, Pennsylvania, United States
[2]Temple university, School of medicine, Philadelphia, Pennsylvania, United States
[3]IRCCS Azienda Ospedaliero-Universitaria di Bologna, Bologna, Italy
[4]Ophthalmology Unit, Dipartimento di Scienze Mediche e Chirurgiche, Alma Mater Studiorum University of Bologna, Bologna, Italy

Correspondence: Jay Chhablani, Department of Ophthalmology, University of Pittsburgh School of Medicine, Pittsburgh, Pennsylvania, 200 Lothrop Street, Pittsburgh, PA 15213, USA; jay.chhablani@gmail.com.

Received: November 24, 2024
Accepted: February 23, 2025
Published: March 25, 2025

Citation: Sadeghi E, Du K, Ajayi O, et al. Three-dimensional choroidal vessels assessment in diabetic retinopathy. *Invest Ophthalmol Vis Sci.* 2025;66(3):50. https://doi.org/10.1167/iovs.66.3.50

Purpose. To evaluate choroidal vasculature in eyes with diabetic retinopathy (DR) using a novel three-dimensional algorithm.

Methods. Patients with DR and healthy controls underwent clinical examinations and swept-source optical coherence tomography (PlexElite-9000). The choroidal layer was segmented using the ResUNet model. Phansalkar thresholding was used to binarize the choroidal vasculature. The macular area was divided into 5 sectors by a custom grid, and the 15 largest vessels in each sector were measured for mean choroidal vessel diameter (MChVD). Volumetric choroidal thickness (ChT) and the choroidal vascularity index (CVI) were calculated. A linear mixed model was used for analysis.

Results. This retrospective cross-sectional study analyzed 73 eyes of 45 patients with DR (36 proliferative vs. 37 nonproliferative DR, and 42 with diabetic macular edema [DME] vs. 31 without DME), and 27 eyes of 21 age-match controls. The average MChVD was decreased in DR compared with healthy (200.472 ± 28.246 µm vs. 240.264 ± 22.350 µm; $P < 0.001$), as well as lower sectoral MChVD ($P < 0.001$); however, there was no difference in average ChT between the groups ($P > 0.05$). The global CVI was reduced in DR, especially in temporal and central sectors ($P < 0.05$). Compared with nonproliferative, proliferative DR exhibited decreased ChT (temporal, $P < 0.05$; other sectors, $P > 0.05$), CVI ($P > 0.05$), and MChVD ($P > 0.05$). DME eyes demonstrated lower but not statistically significant MChVD (196.449 ± 27.221 µm vs. 205.922 ± 29.134 µm; $P > 0.05$) and significantly reduced average CVI (0.365 ± 0.032 vs. 0.389 ± 0.040; $P = 0.008$) compared with non-DME eyes.

Conclusions. DR and DME eyes showed reduced MChVD and CVI, likely owing to microvascular changes leading to ischemia. These findings highlight the need for new choroidal biomarkers to better understand DR's pathogenic mechanisms.

Keywords: diabetic retinopathy, diabetes mellitus, OCT, three-dimensional, choroidal vessel

Diabetes mellitus (DM) leads to vascular complications that cause tissue damage and degeneration.[1] In ophthalmology, the primary concern has been the retinal changes leading to diabetic retinopathy (DR), which is the principal cause of blindness globally, affecting 35% of individuals with diabetes.[2] The retinal damage predominantly involves vascular and neural components, characterized by vessel occlusion and leakage, leukostasis, and disruption of the blood–retinal barrier owing to impaired tight junctions. This process results in increased vascular permeability, free radical generation, mitochondrial dysfunction, neuronal swelling, and apoptosis.[3,4] Initial findings on diabetic choroidopathy revealed choriocapillaris loss, luminal narrowing, thickening of basement membranes with arteriosclerotic alterations in certain arteries, tortuosity of large and intermediate blood vessels, vascular hypercellularity, and the presence of microaneurysms.[5–7]

Optical coherence tomography (OCT) is the primary noninvasive imaging technique for diagnosing and monitoring DR. It offers detailed visualization of retinal changes and diabetic macular edema (DME), assisting in clinical decision-making and patient follow-up.[8] OCT angiography, with its en face imaging, provides insights into vascular abnormalities in the retinal and choroidal vasculatures.[9] Emerging choroidal biomarkers, such as choroidal thickness (ChT), choroidal volume, the choroidal vascularity index (CVI), choroidal vessel layer thickness, and choroidal contour analysis, are enhancing our understanding of choroidal changes

in various diseases.[10–12] Multiple studies have investigated variations in ChT and CVI across different stages of DR using OCT B-scans. The CVI has been identified as an indicator of choroidal dysfunction in type 2 DM.[13,14] It has been shown that the duration of DM is associated with a decrease in the CVI, which in turn is correlated with visual impairment. This finding suggests that the CVI could serve as a dependable biomarker for tracking DR progression.[15] Additionally, OCT angiography studies have revealed significant differences in choroidal perfusion and the volume of large choroidal vessels among patients with varying severity of DR.[16] However, most previous analyses of choroidal vessels have relied on spectral domain OCT and two-dimensional cross-sectional scans. Given the complex, three-dimensional (3D) architecture of choroidal vessels, a 3D evaluation provides a more precise and quantitative analysis.

Our team has developed a validated semiautomated algorithm to reconstruct a 3D image of the choroidal vasculature and measure the diameter of vessels across various segments of the choroid in 3D. We used this method in our recent study to evaluate the choroidal vessel changes in AMD, which helped us to understand the underlying pathogenesis.[17] Our current research aims to use the same method in DR to assess the largest choroidal vessels within the Haller layer compared with age-matched healthy subjects using this innovative 3D approach that helps to gain a better understanding of choroidal vessel changes in this disease. Additionally, we aim to compare choroidal vessels between different stages of DR, including proliferative and nonproliferative disease, as well as the presence of DME.

Material and Methods

Patient Selection

In this retrospective, cross-sectional study, we analyzed the eyes of patients with DR and compared them with healthy controls matched for age and sex. The study was conducted at the Medical Retina and Vitreoretinal Surgery department at the University of Pittsburgh School of Medicine from July 2023 to June 2024. The study adhered to the Declaration of Helsinki guidelines, with a waiver of informed consent obtained owing to its retrospective nature.

The participants in the study were individuals who had been diagnosed with either proliferative or nonproliferative DR, with or without DME. They were categorized based on laboratory data such as hemoglobin A1c and fasting blood sugar levels, as well as thorough fundus examinations conducted by an experienced retina specialist.

We did not include participants with other eye conditions such as vitreoretinal diseases, uveitis, glaucoma, vascular occlusion, AMD, central serous chorioretinopathy, and high myopia. To ensure a more homogenous sample and reliable measurements, we included only patients with a spherical equivalent between −2.5 and 2.5. We also excluded those who had any eye surgeries except for uncomplicated cataract surgeries. Poor-quality OCT scans resulting from eye surface disorders, advanced cataracts, vitreous hemorrhage, opacities, severe sub–internal limiting membrane, or subhyaloid hemorrhage were also considered for exclusion. We performed a power analysis to determine the minimum sample size required to detect significant effects with a desired level of confidence.

OCT Imaging Acquisition

We used the Plex Elite 9000 system by Carl Zeiss Meditec (Dublin, CA, USA) to capture high-resolution images focused on the fovea. The system's expanded field swept-source OCT (SS-OCT) allowed for 12 × 12 mm scans at a 100-kHz acquisition rate. The device can perform scans at a speed of up to 200,000 A-scans per second, using a 1060-nm wavelength. It also has a tissue penetration depth of up to 6 mm and an axial resolution of approximately 6.3 µm.

We assessed the scan quality using the SS-OCT software's built-in scoring system. Only scans with a score of 6 or higher out of 10, which is shown in green, were included in our analysis. These SS-OCT scans were exported as 8-bit volumes, each containing 1024 B-scans with a resolution of 1024 × 1536 pixels. After the acquisition, we reviewed the multimodal imaging data. A retina specialist categorized eyes with DR into proliferative and nonproliferative stages, as well as those with or without DME.

Automated Choroidal Vessel Segmentation

The methodology described combines automated and manual techniques to measure the 3D cross-sectional diameter of choroidal vessels. We used the same method as our recently published paper on AMD,[17] and another recent publication on healthy eyes.[18] We start by using a ResUnet, a type of deep learning architecture, to outline the boundaries of the choroid in structural SS-OCT scans.[19] This process involves identifying the choroid inner boundary at the junction of the RPE and choriocapillaris, as well as the choroid outer boundary at the choroidal–scleral junction. Choroidal segmentation was done using a deep learning model and then smoothed volumetrically, with manual boundary correction applied to address any potential issues.[19–21] The deep learning model, detailed in our unpublished research, achieved a 93% accuracy in delineating choroidal boundaries, which improved to 100% after manual correction.

The next step in our process was to separate the choroidal blood vessels from SS-OCT volumes. Because OCT image acquisition presents challenges like speckle noise, retinal shadows, contrast fluctuations, and misalignment of B-scans, as well as the complex architecture and intensity characteristics of choroidal blood vessels, we used the Phansalkar thresholding method to distinguish between luminal and stromal areas.[22–24]

Traditional intensity-based thresholding techniques often struggle to segment vessels accurately owing to artifacts and complexities. To overcome this limitation, our group has developed the Phansalkar thresholding method, which dynamically calculates local thresholds within each 16 × 16 pixel tile across the B-scans, enabling clear differentiation between luminal and stromal areas.[22] Subsequently, morphological postprocessing is applied to eliminate unnecessary elements, resulting in a seamlessly constructed 3D model of the choroidal vasculature.

We have created two graphical user interfaces to make both automated and manual tasks easier in our proposed method. The first graphical user interface is specifically made for accurately extracting 3D choroidal vasculature from OCT data. It can handle raw SS-OCT volumes in .IMG or .JPG formats and assist in segmenting choroid boundaries and vessels. If needed, manual correction of choroidal segmentation is also possible.

Investigative Ophthalmology & Visual Science

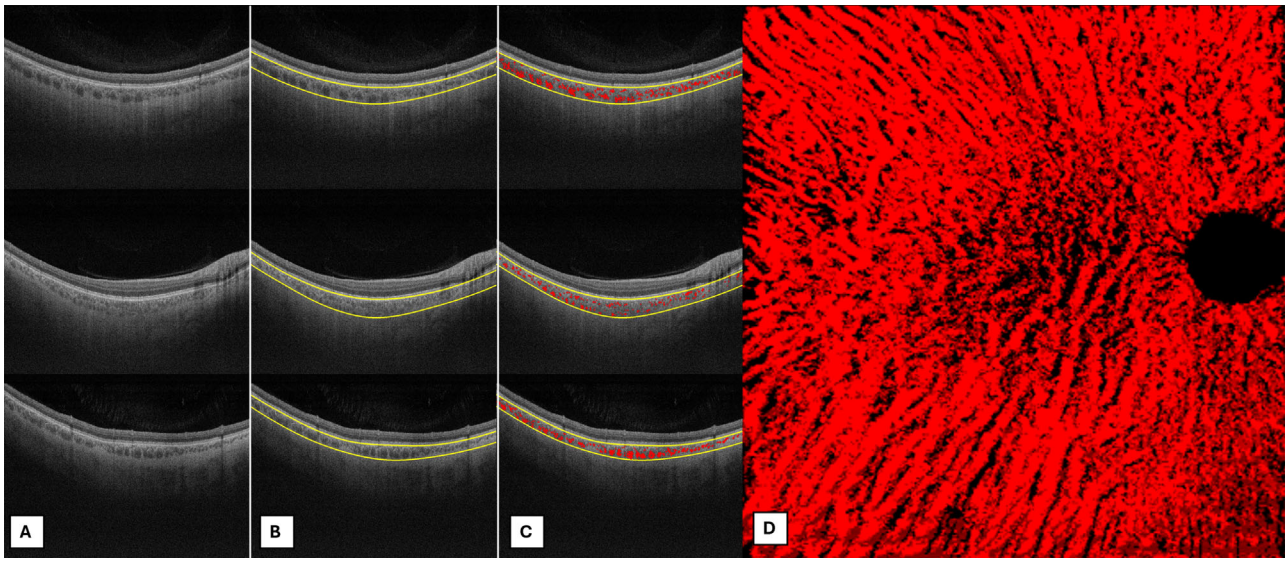

Figure 1. Process of segmenting choroidal boundaries and vessels, followed by the reconstruction of a 3D choroidal vessel view. (**A**) Three SS-OCT scans from a cube scan of the right eye of a healthy individual. (**B**) Choroidal segmentation at the choroid inner boundary, located at the junction of the RPE layer, and choriocapillaris, and the choroid outer boundary at the choroidal-scleral junction. (**C**) Automated segmentation of choroidal vessels. (**D**) Reconstructed 3D, 12 × 12 mm choroidal vessel map with a masked optic disc. All these steps are performed using the first graphical user interface.

We used ImageJ 1.51 s (National Institutes of Health, Bethesda, MD, USA) to make a mask of the optic disc. This mask is then used to hide the blood vessels in the choroid at the optic disc locations. After this, we segment the choroid vessels and save the resulting 3D models of the choroidal vasculature for later manual measurement of cross-sectional diameters (Fig. 1).

To measure the ChT, CVI, and cross-sectional vessel diameters, the datasets are imported into the second graphical user interface. This interface allows the grader to select any volume by identifying the center of the fovea in the RPE en face image, which corresponds with the center of the foveal avascular zone in the cross-sectional B-scan. A 12 × 12 grid is then applied over the 3D choroidal vasculature, highlighting different sectors: central, nasal, temporal, superior, and inferior. The central sector is defined by a 4-mm diameter circle (Fig. 2).

Our algorithm was able to segment the entire choroid, but it had difficulty in defining and reconstructing the choriocapillaris vessels. As a result, the 3D vessel reconstruction was only possible for Sattler's and Haller's vessels. This study specifically examined the largest vessels (>100 microns) in each sector, all of which belonged to the Haller layer.[12,25,26]

Assessment of Choroidal Vessel Diameter

Selecting a point on the 3D map brings up a window showing the vasculature in a small, fixed-size view around that point. The grader can rotate the vasculature to get the best view of the vessels for accurate measurements. The cross-sectional diameter was measured from the outermost visible portions of each vessel, with one measurement taken at the thickest part of each vessel. The average of these 15 measurements was then calculated to determine the mean choroidal vessel diameter (MChVD) for each sector (Fig. 3).

To evaluate the intraclass correlation coefficient (ICC), two masked readers (E.S. and K.D.), who were unaware of the patients' details, performed measurements across all sectors for 10 eyes. A total of 750 measurements taken by the second reader (K.D.) were used to assess inter-reader reliability, and the measurements taken by the first reader (E.S.) were used for this study. The ChT and the CVI for the entire volume were determined using the ResUnet and Phansalkar thresholding methods.

Statistical Analysis

Data normality was assessed using the Shapiro–Wilk test, followed by parametric testing. The consistency between raters for image binarization was evaluated using the absolute agreement model of the ICC. The ICC values were interpreted as follows: (1) Less than 0.5 indicated poor reliability; (2) 0.5 to 0.75 suggested moderate reliability; (3) 0.75 to 0.9 denoted good reliability; and (4) values greater than 0.90 signified excellent reliability. For categorical data analysis, the χ^2 test was applied. Demographic data, ChT, CVI, and MChVD were compared across predefined groups using linear mixed models. These groups included DR vs. age- and sex-matched healthy patients, proliferative vs. nonproliferative DR, and eyes with vs. without DME, as outlined in the study design. Because these comparisons were planned primary analyses and not exploratory or post hoc tests, adjustments for multiple tests were not applied. In addition, linear mixed models were used in the statistical analysis to account for the correlation between the two eyes of each patient. Patient ID was set as a random effect, helping to account for the inherent correlation in our data. A P value of less than 0.05 was considered statistically significant. To address the issue of multiple comparisons, we applied Bonferroni correction. All statistical analyses were conducted using IBM's Statistical Package for Social Sciences (SPSS) version 26 (IBM, Inc, Armonk, NY, USA).

Investigative Ophthalmology & Visual Science

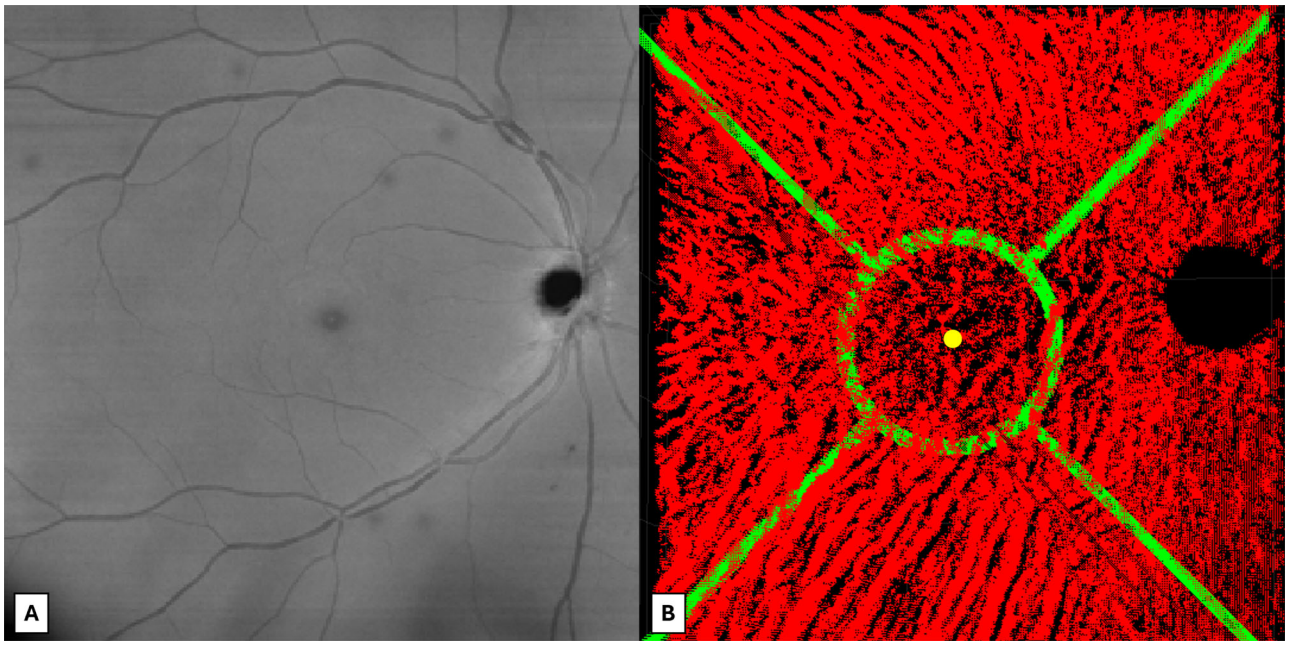

Figure 2. How to delineate various sectors, including nasal, temporal, superior, inferior, and central, in a 3D choroidal vessel map. (**A**) RPE en face OCT. (**B**) Different sectors based on the center of the fovea (center of the foveal avascular zone on RPE enface image). All these steps are performed using the second graphical user interface.

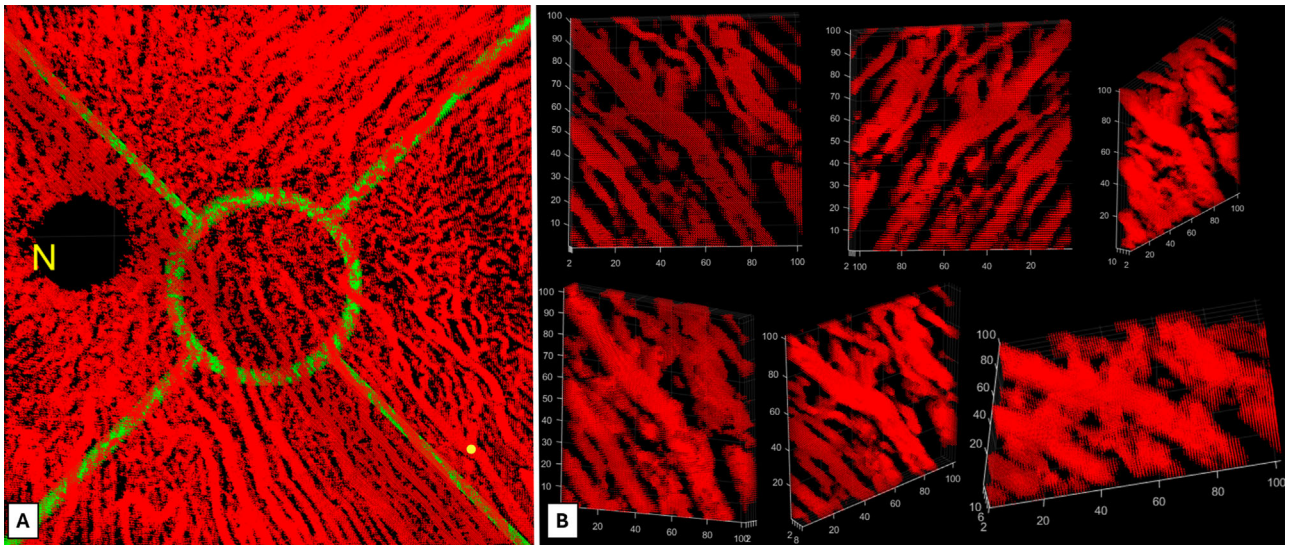

Figure 3. Process of selecting a vessel for measurement. (**A**) A vessel in the temporal sector, indicated by a *yellow circle*. (**B**) By clicking on this vessel, a zoomed 3D image appears, which can be rotated 360° in all planes. This allows the user to rotate the image and choose the optimal view for accurate measurement. As an example, the selected vessel has a 285.89-micron diameter. The same procedure is done for the 15 largest vessels in each sector. N, nasal.

Results

Demographic Data

In our analysis, we examined 100 eyes from 66 individuals. Among the 45 patients with DR, 28 individuals included both eyes, and 17 patients included only 1 eye because of a poor-quality scan of fixation loss in 13 eyes, vascular accident in 2 eyes, and anterior ischemic optic neuropathy in 2 eyes. Within the healthy group, 6 individuals included both eyes, and the remaining 15 included 1 eye each, because of low-quality OCT owing to cataract in 4 eyes and fixation loss in 11 eyes. A total of 73 eyes of 45 patients with DR and 27 eyes of 21 healthy, age and sex-matched controls were included in this study.

The average age of the individuals was 60.50 ± 15.08 years, with 33 females (50.00%). There were no significant age differences observed between patients with DR and healthy subjects (61.22 ± 11.87 years vs. 59.00

Investigative Ophthalmology & Visual Science

Table 1. Demographic Data

	Total (100 Eyes, 66 Subjects)	DR (73 Eyes, 45 Patients)	Healthy (27 Eyes, 21 Subjects)	*P* Value
Age (years)	60.507 ± 15.083	61.227 ± 11.871	59.000 ± 20.530	0.582
Female	33 (50.00%)	21 (46.66%)	12 (57.14%)	0.944
Right eye	55 (55.00%)	39 (53.42%)	16 (59.25%)	0.607
BCVA (LogMAR)	0.276 ± 0.328	0.375 ± 0.433	0.017 ± 0.036	**<0.001**

BCVA, best-corrected visual acuity
P values < 0.05 are shown in bold text.
Values are mean ± standard deviation or number (%).

Table 2. Comparison of Choroidal Parameters Between Eyes Affected by DR Vs. Healthy Controls

	DR (73 Eyes)	Healthy (27 Eyes)	*P* Value	Confidence Interval	Beta Coefficient
MChVD (µm)					
Average MChVD	200.472 ± 28.246	240.264 ± 22.350	**<0.001**	229.370–251.889	240.630
Nasal MChVD	195.559 ± 37.013	228.498 ± 23.405	**<0.001**	214.466–242.776	228.621
Temporal MChVD	201.496 ± 31.269	247.790 ± 31.836	**<0.001**	235.437–261.398	248.418
Inferior MChVD	207.513 ± 32.312	255.944 ± 29.889	**<0.001**	242.891–268.908	255.900
Superior MChVD	210.024 ± 34.157	251.268 ± 30.244	**<0.001**	238.558–266.685	252.621
Central MChVD	187.768 ± 28.337	216.990 ± 27.392	**<0.001**	204.873–228.316	216.594
ChT (µm)					
Average ChT	217.688 ± 53.991	216.934 ± 45.607	0.948	196.936–236.926	216.931
Nasal ChT	188.835 ± 52.078	198.551 ± 64.476	0.460	176.791–220.939	198.866
Temporal ChT	213.979 ± 48.961	218.887 ± 44.109	0.649	200.662–237.113	218.887
Inferior ChT	236.950 ± 56.130	226.140 ± 45.962	0.374	205.340–246.775	226.058
Superior ChT	205.506 ± 62.123	199.852 ± 50.964	0.673	177.179–222.525	199.852
Central ChT	243.173 ± 73.716	245.435 ± 55.663	0.890	218.065–273.027	245.546
CVI (%)					
Average CVI	0.375 ± 0.037	0.394 ± 0.038	**0.029**	0.380–0.409	0.394
Nasal CVI	0.356 ± 0.055	0.375 ± 0.055	0.166	0.353–0.397	0.375
Temporal CVI	0.362 ± 0.041	0.390 ± 0.042	**0.005**	0.274–0.407	0.390
Inferior CVI	0.394 ± 0.037	0.403 ± 0.047	0.360	0.387–0.420	0.403
Superior CVI	0.387 ± 0.046	0.397 ± 0.043	0.367	0.379–0.416	0.397
Central CVI	0.375 ± 0.041	0.404 ± 0.035	**0.002**	0.389–0.420	0.405

P values < 0.05 are shown in bold text.

± 20.53 years; $P = 0.582$). There were no significant sex differences between the groups, with (21 females (46.66%) among patients with DR vs. 12 among the healthy individuals (57.14%); $P = 0.944$). Best-corrected visual acuity was significantly lower in DR eyes compared with controls (0.375 ± 0.433 logMAR vs. 0.017 ± 0.036 logMAR; $P < 0.001$). Among the 73 diabetic eyes analyzed, 36 were classified as proliferative, and 37 were nonproliferative. Additionally, 42 eyes exhibited DME, whereas 31 did not. Furthermore, 30 eyes were treated with panretinal photocoagulation, 29 eyes received intravitreal anti-VEGF injections, and 15 eyes were administered intravitreal dexamethasone implants (Table 1).

Three-dimensional Assessment in DR Vs. Healthy Eyes

An assessment of 10 eyes (150 choroidal vessels) for ICC between two masked readers for measurements of MChVD demonstrated a high level of agreement across all sectors, with an ICC value of 0.892 and a confidence interval ranging from 0.811 to 0.933. After applying Bonferroni correction, the *P* value of less than 0.0167 was statistically significant.

Comparing eyes with DR to healthy controls revealed no significant difference in global or per-sector ChT (average ChT in DR, 217.688 ± 53.991 µm vs. average ChT in healthy, 216.934 ± 45.607 µm; $P = 0.948$). However, CVI was significantly decreased in DR (average CVI in DR, 0.375 ± 0.037 vs. average CVI in healthy, 0.394 ± 0.038; $P = 0.029$), particularly in the global, temporal, and central sectors ($P < 0.05$).

In evaluating MChVD, results showed a strong and significant reduction in DR eyes compared with healthy eyes, both globally (average MChVD in DR, 200.472 µm ± 28.246 µm vs. average MChVD in healthy eyes, 240.264 µm ± 22.350 µm; $P < 0.001$) and across all sectors ($P < 0.001$) (Table 2). A representative example is shown in Figure 4.

Three-dimensional Assessment in Proliferative Vs. Nonproliferative DR

The comparison between 36 eyes with proliferative DR and 43 eyes with nonproliferative DR indicated a nonstatistically significant reduced ChT in proliferative DR globally (average ChT in proliferative DR, 209.102 µm ± 223.679 µm vs. nonproliferative, 223.679 µm ± 61.356 µm; $P = 0.259$), as well as sectors ($P > 0.05$). Choroidal thinning was statistically significant in the temporal sector in eyes with proliferative DR in comparison with nonproliferative (202.570 µm ± 44.577 µm vs. 225.080 ± 51.046 µm; $P = 0.049$).

Investigative Ophthalmology & Visual Science

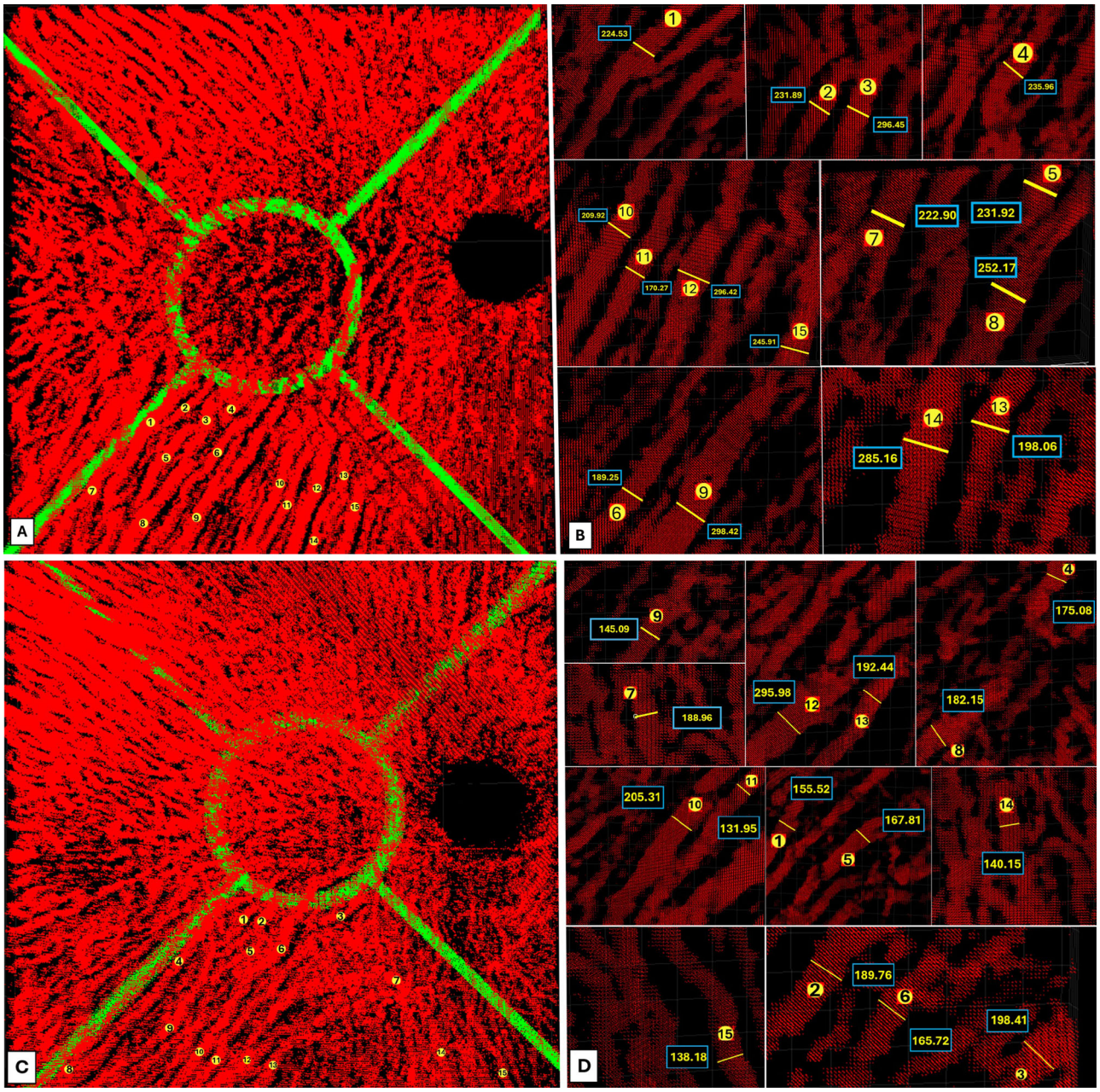

Figure 4. Assessment of the MChVD in the inferior sector of the right eye in a 59-year-old healthy male (**A**, **B**) and an eye with nonproliferative DR in a 60-year-old diabetic male (**C**, **D**). (**A**) The thickest part of the 15 largest vessels from the inferior sector of a healthy eye are labeled with *yellow circles*. (**B**) By selecting the best view of the vessels, the MChVD is measured for each of the 15 vessels. The average MChVD in the inferior sector is 239.28 microns. (**C**) The 15 largest vessels from the inferior sector of an eye with nonproliferative DR are labeled with *yellow circles*. (**D**) The average MChVD for the largest 15 vessels is 178.16 microns.

A decreased MChVD and CVI were seen globally and in each sector, which was not statistically significant ($P > 0.05$) (Table 3).

Three-dimensional Assessment in DR With DME Vs. DR Without DME

The analysis between 42 eyes with DR and DME (including 21 proliferative DR and 21 nonproliferative DR) and 31 eyes with DR and without DME (including 15 proliferative DR and 16 nonproliferative DR) revealed that eyes with DME had a lower CVI globally (DR with DME, 0.365 ± 0.032 vs. DR without DME, 0.389 ± 0.040; $P = 0.008$). This difference was statistically significant, particularly in the temporal, inferior, and superior sectors ($P < 0.05$). No significant differences were observed in ChT between these two subgroups. Additionally, MChVD showed a reduction in DME globally that was not statistically significant (DR with DME, 196.449 ± 27.221 µm vs. DR without DME, 205.922 ± 29.134 µm; $P = 0.843$) and across all sectors ($P > 0.05$) (Table 4).

Investigative Ophthalmology & Visual Science

Table 3. Comparison of Choroidal Parameters Between Eyes Affected by Proliferative vs. Nonproliferative DR

	Proliferative DR (36 Eyes)	Nonproliferative DR (37 Eyes)	*P* Value	Confidence Interval	Beta Coefficient
MChVD (µm)					
Average MChVD	197.274 ± 28.799	203.584 ± 27.734	0.934	190.987–212.180	201.583
Nasal MChVD	188.717 ± 38.6	202.215 ± 34.344	0.337	187.063–214.482	200.772
Temporal MChVD	198.724 ± 34.561	204.193 ± 27.911	0.658	192.418–215.119	203.769
Inferior MChVD	205.566 ± 32.171	209.406 ± 34.615	0.896	196.787–220.522	208.654
Superior MChVD	206.537 ± 30.984	213.418 ± 37.094	0.820	197.035–222.805	209.920
Central MChVD	186.825 ± 24.704	188.685 ± 31.794	0.730	179.630–197.256	186.943
ChT (µm)					
Average ChT	207.884 ± 37.289	227.227 ± 65.488	0.127	209.697–244.758	227.228
Nasal ChT	187.455 ± 36.538	190.178 ± 64.208	0.866	172.165–207.961	190.063
Temporal ChT	202.570 ± 44.577	225.080 ± 51.046	**0.049**	209.357–240.804	225.080
Inferior ChT	224.268 ± 40.495	249. 288 ± 66.256	0.056	231.231–267.345	249.288
Superior ChT	198.101 ± 48.285	212.710 ± 73.102	0.319	192.348–233.074	212.711
Central ChT	227.027 ± 47.335	258.882 ± 90.418	0.064	235.131–282.633	258.882
CVI (%)					
Average CVI	0.371 ± 0.035	0.379 ± 0.039	0.359	0.367–0.392	0.380
Nasal CVI	0.345 ± 0.049	0.368 ± 0.060	0.102	0.349–0.388	0.368
Temporal CVI	0.355 ± 0.038	0.368 ± 0.043	0.207	0.355–0.382	0.368
Inferior CVI	0.389 ± 0.035	0.390 ± 0.014	0.236	0.387–0.414	0.400
Superior CVI	0.380 ± 0.049	0.395 ± 0.049	0.190	0.379–0.412	0.395
Central CVI	0.371 ± 0.047	0.372 ± 0.036	0.540	0.359–0.386	0.372

P values < 0.05 are shown in bold text.

Table 4. Comparison of Choroidal Parameters Between Eyes Affected by DME or Not in Eyes With DR

	DR With DME (42 Eyes)	DR Without DME (31 Eyes)	*P* Value	Confidence Interval	Beta Coefficient
MChVD (µm)					
Average MChVD	196.449 ± 27.221	205.922 ± 29.134	0.843	191.018–210.400	200.709
Nasal MChVD	190.802 ± 34.623	202.003 ± 39.685	0.656	181.948–207.310	194.629
Temporal MChVD	199.942 ± 33.903	203.602 ± 27.709	0.936	191.250–212.320	201.785
Inferior MChVD	203.670 ± 32.385	212.719 ± 32.221	0.614	195.517–217.201	206.359
Superior MChVD	204. 399 ± 32.562	217.646 ± 35.308	0.839	198.438–221.899	210.168
Central MChVD	183.434 ± 27.009	193.640 ± 29.466	0.302	175.787–194.403	185.095
ChT (µm)					
Average ChT	216.165 ± 54.482	219.752 ± 54.146	0.781	199.446–232.885	216.165
Nasal ChT	187.455 ± 56.475	190.705 ± 46.304	0.790	170.885–204.278	187.581
Temporal ChT	213.711 ± 48.172	214.343 ± 50.809	0.957	198.542–228.881	213.711
Inferior ChT	234.758 ± 51.016	239.919 ± 63.156	0.712	217.152–252.529	234.841
Superior ChT	203.075 ± 66.380	208.800 ± 56.753	0.700	183.848–222.303	203.075
Central ChT	241.828 ± 73.912	244.995 ± 74.630	0.846	218.472–265.157	241.814
CVI (%)					
Average CVI	0.365 ± 0.032	0.389 ± 0.040	**0.008**	0.355–0.377	0.366
Nasal CVI	0.348 ± 0.047	0.367 ± 0.063	0.183	0.330–0.367	0.349
Temporal CVI	0.352 ± 0.036	0.375 ± 0.043	**0.021**	0.340–0.365	0.353
Inferior CVI	0.382 ± 0.029	0.410 ± 0.041	**0.002**	0.371–0.394	0.382
Superior CVI	0.374 ± 0.040	0.403 ± 0.049	**0.009**	0.358–0.389	0.374
Central CVI	0.368 ± 0.042	0.384 ± 0.038	0.114	0.356–0.382	0.369

P values < 0.05 are shown in bold text.

Discussion

Using a novel algorithm for the 3D assessment of choroidal vessels, we found that the MChVD was significantly lower in eyes with DR compared with healthy eyes (200.472 ± 28.246 µm vs. 240.264 ± 22.350 µm; $P < 0.001$). The MChVD in all the sectors significantly reduced in eyes with DR ($P < 0.001$). Additionally, the CVI was reduced in eyes with DR, particularly in the global, temporal, and central sectors ($P < 0.05$). Eyes with PDR demonstrated a nonsignificant decreased ChT (temporal sector, $P < 0.05$; other sectors, $P > 0.05$), decreased MChVD ($P > 0.05$), and decreased CVI ($P > 0.05$) compared with eyes with NPDR. Eyes with DME showed a nonsignificant decreased MChVD ($P > 0.05$) and ChT ($P > 0.05$), and significantly reduced CVI in the average, temporal, inferior, and superior sectors ($P < 0.05$) compared with eyes without DME.

This study used a novel validated semiautomated algorithm to create 3D visualizations of choroidal vessels. This new tool allowed us to measure the diameters of large choroidal vessels accurately within a 3D framework, which helped us to analyze the choroidal vasculature thoroughly in patients with DR. Previous studies on the choroid have mainly concentrated on 2D B-scans.[11,27] Given the variability of depth and 3D positioning, measurements obtained from 2D or en face imaging are inherently unreliable. Most of

Investigative Ophthalmology & Visual Science

the previous studies focused on the vascular changes in the choriocapillaris based on the OCT angiography data[28–30]; however, our findings globally relate to the attenuation of the choroidal medium and large vascular networks in the Sattler and Haller layers derived from structural data. Therefore, 3D analysis is crucial for a more accurate assessment of choroidal vessels, leading to a deeper understanding of disease pathophysiology.

Previous studies have examined the relationship between ChT and the presence of DM, with or without DR, of varying severities, which exhibited inconsistent results.[31–36] A meta-analysis by Endo et al.[31] that included 17 related studies found that subfoveal ChT was thinner in diabetic eyes without DR compared with healthy eyes. Another study by Xu et al.[32] reported that patients with DM showed a slightly thicker choroid compared with healthy eyes. In the presence of DR, some studies indicated that a greater severity of DR showed a thinner ChT.[33–35] Wang et al.[36] reported that the ChT increased in the early stages of DR and then decreased as DR progressed, but the presence of DME was not associated significantly with ChT. However, this association was not observed in the Beijing Eye Study, which was based on a population sample. They found that patients with DM had slightly increased ChT; however, DR in different stages did not affect the ChT.[32] Kinoshita et al.[37] found that the choroidal lumen and stroma may increase as DR progresses. We found no significant difference in ChT between eyes with DR and healthy eyes; additionally, we noted a nonsignificant reduction in the proliferative stage and eyes with DME. A decrease in the ChT leads to decreased blood flow in the choroid, compromising the supply of oxygen and nutrients to the retinal tissues. This process can contribute to ischemia, which may accelerate the progression of DR. This relationship highlights the importance of monitoring ChT in patients with DR.

Different studies have shown the correlation of CVI with DM with or without DR.[15] Keskin et al.[38] observed that CVI is generally lower in patients with diabetes, with a more pronounced decrease in those with DR. They proposed that CVI could act as a sensitive and early indicator for the onset of DR.[38] A negative correlation between CVI and the severity of DR was reported.[39–41] A study by Aksoy et al.[14] on patients with type 1 DM without DR demonstrated that CVI could serve as an indicator of subclinical choroidal dysfunction in these patients. They reported no significant differences in ChT, total choroidal area, lumina, and stromal area between healthy patients and patients with diabetes. However, patients with type 1 DM exhibited significantly reduced CVI compared with healthy controls, with a negative correlation observed between CVI and disease duration.[14] Our study found that the CVI was decreased significantly in eyes with DR compared with healthy eyes. We also observed a reduction in CVI in eyes with DME. Additionally, there was a nonsignificant reduced CVI in proliferative DR. We demonstrated that CVI is correlated with both the occurrence and severity of disease, suggesting its potential as a predictive biomarker in DR. Increasing choroidal stromal volume owing to inflammation or extracellular fluid accumulation and decreasing vessel volume owing to choroidal blood flow deficit along with vessel constriction may play a role in a decrease in the CVI during disease progression.

During DR progression, choroidal vessel diameter may decrease owing to vascular constriction from choroidal hypoxia, with changes in blood flow occurring before retinopathy manifests.[42,43] A study conducted by Muir et al.[44] investigated choroidal and retinal blood flow in Ins2Akita models using magnetic resonance imaging. The findings revealed that a deficit in choroidal blood flow was detected 5 months earlier than changes in retinal blood flow and decreases in visual acuity. This early decrease in choroidal blood flow may offer a way to assess the onset of early DR before significant damage or progression to proliferative retinopathy.[44] Other studies indicated that choroidal volume and blood flow are significantly reduced in patients with proliferative DR,[45] especially those with DME.[43] Our study revealed a significant reduction in the MChVD in eyes with DR compared with healthy eyes. Additionally, we observed a nonsignificant reduced MChVD in eyes with DME. The application of this advanced 3D method for measuring the diameter of large choroidal vessels may serve as a novel biomarker for the detection and progression of DR.

Our study had some limitations owing to its retrospective and cross-sectional design and limited sample size; a larger sample size could provide more detailed results. The cross-sectional approach also prevented us from tracking the progressive choroidal changes in patients with DR over time, which is important for a better understanding of the choroidal role in DR. Owing to the lack of delineation of choriocapillaris, 3D reconstruction was limited to Sattler's and Haller's vessels, focusing on the largest ones (>100 microns) in each sector.[12,25,26] Without adjustment for axial length, angular units like arcminutes or degrees would be ideal, but we are unable to use these scales during postprocessing analysis.[46,47] Further research using 3D imaging is necessary to gain deeper insights into choroidal changes in DR, which our team aims to explore in future experiments.

Conclusions

This study found that in eyes affected by DR, the MChVD, ChT, and CVI exhibited changes associated with disease occurrence and progression. Specifically, CVI and MChVD were decreased in DR eyes compared with healthy controls. Additionally, eyes with DME displayed reduced CVI and MChVD. The use of 3D choroidal imaging offers a novel, noninvasive approach to examining choroidal vessel changes in DR and other ocular diseases. This method may significantly enhance our understanding of the underlying mechanisms driving pathogenesis. Future research could facilitate automated measurements of vessel diameters, vessel positioning, and other choroidal vascular features in 3D images at all stages of DR. These measurements hold potential as imaging markers for identifying patients at risk, early detection, and disease progression.

Acknowledgments

Supported by an NIH CORE Grant P30 EY08098 to the Department of Ophthalmology, the Eye and Ear Foundation of Pittsburgh, and from an unrestricted grant from Research to Prevent Blindness, New York, New York.

Disclosure: **E. Sadeghi**, None; **K. Du**, None; **O. Ajayi**, None; **E. Davis**, None; **N. Valsecchi**, None; **M.N. Ibrahim**, None; **S.C. Bollepalli**, NetraMind Innovations (I); **K.K. Vupparaboina**, NetraMind Innovations (I); **J.A. Sahel,** NetraMind Innovations (I), Pixium Vision (I), GenSight Biologics (I), Sparing Vision (I), Prophesee (I), Chronolife (I); **J. Chhablani**, NetraMind Innovations (O), Allergan (C), Novartis (C), Salutaris (C), OD-OS (C),

Erasca (C), B&L (C), Iveric Bio (C), Ocular Therapeutics (I), AcuViz (I), Abbvie (I), Springer (R), Elsevier (R)

References

1. Li Y, Liu Y, Liu S, et al. Diabetic vascular diseases: Molecular mechanisms and therapeutic strategies. *Signal Transduct Target Ther*. 2023;8(1):152.
2. Yau JW, Rogers SL, Kawasaki R, et al. Global prevalence and major risk factors of diabetic retinopathy. *Diabetes Care*. 2012;35(3):556–564.
3. Antonetti DA, Klein R, Gardner TW. Mechanisms of disease diabetic retinopathy. *N Engl J Med*. 2012;366(13):1227–1239.
4. Lutty GA. Diabetic choroidopathy. *Vision Res*. 2017;139:161–167.
5. Hidayat AA, Fine BS. Diabetic choroidopathy: Light and electron microscopic observations of seven cases. *Ophthalmology*. 1985;92(4):512–522.
6. Fryczkowski AW, Hodes BL, Walker J. Diabetic choroidal and iris vasculature scanning electron microscopy findings. *Int Ophthalmol*. 1989;13(4):269–279.
7. Fryczkowski AW, Hodes BL, Walker J. Diabetic choroidal and iris vasculature scanning electron microscopy findings. *Int Ophthalmol*. 1989;13:269–279.
8. Virgili G, Menchini F, Casazza G, et al. Optical coherence tomography (OCT) for detection of macular oedema in patients with diabetic retinopathy. *Cochrane Database Syst Rev*. 2015;1(1):CD008081.
9. Chua J, Sim R, Tan B, et al. Optical coherence tomography angiography in diabetes and diabetic retinopathy. *J Clin Med*. 2020;9(6):1723.
10. Zarnegar A, Valsecchi N, Sadeghi E, et al. Choroidal imaging biomarkers as predictors of conversion to exudative age-related macular degeneration. *Graefes Arch Clin Exp Ophthalmol*. 2024;263:1–9.
11. Ruiz-Moreno JM, Gutiérrez-Bonet R, Chandra A, Vupparaboina KK, Chhablani J, Ruiz-Medrano J. Choroidal vascularity index versus choroidal thickness as biomarkers of acute central serous chorioretinopathy. *Ophthalm Res*. 2023;66(1):615–623.
12. Singh SR, Vupparaboina KK, Goud A, Dansingani KK, Chhablani J. Choroidal imaging biomarkers. *Surv Ophthalmol*. 2019;64(3):312–333.
13. Adhi M, Brewer E, Waheed NK, Duker JS. Analysis of morphological features and vascular layers of choroid in diabetic retinopathy using spectral-domain optical coherence tomography. *JAMA Ophthalmol*. 2013;131(10):1267–1274.
14. Aksoy M, Simsek M, Apaydın M. Choroidal vascularity index in patients with type-1 diabetes mellitus without diabetic retinopathy. *Current Eye Res*. 2021;46(6):865–870.
15. Jing R, Sun X, Cheng J, Li X, Wang Z. Vascular changes of the choroid and their correlations with visual acuity in diabetic retinopathy. *Front Endocrinol*. 2024;15:1327325.
16. Liu T, Lin W, Shi G, et al. Retinal and choroidal vascular perfusion and thickness measurement in diabetic retinopathy patients by the swept-source optical coherence tomography angiography. *Front Med*. 2022;9:786708.
17. Sadeghi E, Valsecchi N, Ibrahim MN, et al. Three-dimensional choroidal vessels assessment in age-related macular degeneration. *Invest Ophthalmol Vis Sci*. 2024;65(13):39.
18. Valsecchi N, Sadeghi E, Davis E, et al. Assessment of choroidal vessels in healthy eyes using 3-dimensional vascular maps and a semi-automated deep learning approach. *Sci Rep*. 2025;15(1):714.
19. Arora S, Singh SR, Rosario B, et al. Three-dimensional choroidal contour mapping in healthy population. *Sci Rep*. 2024;14(1):6210.
20. Vupparaboina KK, Selvam A, Suthaharan S, et al. Automated choroid layer segmentation based on wide-field ss-oct images using deep residual encoder-decoder architecture. *Invest Ophthalmol Vis Sci*. 2021;62(8):2162.
21. Jana S. Volumetric quantification of choroid and Haller's sublayer using OCT scans: An accurate and unified approach based on stratified smoothing. *Compute Med Imaging Graph*. 2022;99:102086..
22. Ibrahim MN, Bollepalli SC, Selvam A, et al. Accurate detection of 3D choroidal vasculature using swept-source OCT volumetric scans based on phansalkar thresholding. *2023 IEEE EMBS International Conference on Biomedical and Health Informatics (BHI)*. Pittsburgh, PA; IEEE; 2023.
23. Agrawal R, Seen S, Vaishnavi S, et al. Choroidal vascularity index using swept-source and spectral-domain optical coherence tomography: A comparative study. *Ophthalmic Surg Lasers Imaging Retina*. 2019;50(2):e26–e32.
24. Vupparaboina KK, Richhariya A, Chhablani JK, Jana S. Optical coherence tomography imaging: Automated binarization of choroid for stromal-luminal analysis. *2016 International Conference on Signal and Information Processing (IConSIP)*. Washington, DC: IEEE; 2016:1–5.
25. Shiihara H, Sonoda S, Terasaki H, et al. Quantification of vessels of Haller's layer based on en-face optical coherence tomography images. *Retina*. 2021;41(10):2148–2156.
26. Esmaeelpour M, Kajic V, Zabihian B, et al. Choroidal Haller's and Sattler's layer thickness measurement using 3-dimensional 1060-nm optical coherence tomography. *PloS One*. 2014;9(6):e99690.
27. Breher K, Terry L, Bower T, Wahl S. Choroidal biomarkers: a repeatability and topographical comparison of choroidal thickness and choroidal vascularity index in healthy eyes. *Transl Vis Sci Technol*. 2020;9(11):8.
28. Nesper PL, Roberts PK, Onishi AC, et al. Quantifying microvascular abnormalities with increasing severity of diabetic retinopathy using optical coherence tomography angiography. *Invest Ophthalmol Vis Sci*. 2017;58(6):BIO307–BIO315.
29. Dai Y, Zhou H, Chu Z, et al. Microvascular changes in the choriocapillaris of diabetic patients without retinopathy investigated by swept-source OCT angiography. *Invest Ophthalmol Vis Sci*. 2020;61(3):50.
30. Forte R, Haulani H, Jürgens I. Quantitative and qualitative analysis of the three capillary plexuses and choriocapillaris in patients with type 1 and type 2 diabetes mellitus without clinical signs of diabetic retinopathy: a prospective pilot study. *Retina*. 2020;40(2):333–344.
31. Endo H, Kase S, Saito M, et al. Choroidal thickness in diabetic patients without diabetic retinopathy: A meta-analysis. *Am J Ophthalmol*. 2020;218:68–77.
32. Xu J, Xu L, Du KF, et al. Subfoveal choroidal thickness in diabetes and diabetic retinopathy. *Ophthalmology*. 2013;120(10):2023–2028.
33. Horváth H, Kovács I, Sándor GL, et al. Choroidal thickness changes in non-treated eyes of patients with diabetes: swept-source optical coherence tomography study. *Acta Diabetol*. 2018;55(9):927–934.
34. Ambiya V, Kumar A, Baranwal VK, et al. Change in subfoveal choroidal thickness in diabetes and in various grades of diabetic retinopathy. *Int J Retina Vitreous*. 2018;4:34.
35. Laíns I, Talcott KE, Santos AR, et al. Choroidal thickness in diabetic retinopathy assessed with swept-source optical coherence tomography. *Retina*. 2018;38(1):173–182.
36. Wang W, Liu S, Qiu Z, et al. Choroidal thickness in diabetes and diabetic retinopathy: A swept source OCT study. *Invest Ophthalmol Vis Sci*. 2020;61(4):29.

Investigative Ophthalmology & Visual Science

37. Kinoshita T, Imaizumi H, Shimizu M, et al. Systemic and ocular determinants of choroidal structures on optical coherence tomography of eyes with diabetes and diabetic retinopathy. *Sci Rep*. 2019;9(1):16228.
38. Keskin Ç, Dilekçi E, Üçgül A, Üçgül R, Toprak G, Cengiz D. Choroidal vascularity index as a predictor for the development of retinopathy in diabetic patients. *J Endocrinol Invest*. 2024;47(5):1175–1180.
39. Wang X, Li R, Chen J, et al. Choroidal vascularity index (CVI)-Net-based automatic assessment of diabetic retinopathy severity using CVI in optical coherence tomography images. *J Biophotonics*. 2023;16(6):e202200370.
40. Nicolini N, Tombolini B, Barresi C, et al. Assessment of diabetic choroidopathy using ultra-widefield optical coherence tomography. *Transl Vis Sci Technol*. 2022;11(3):35.
41. Han X, Du N-N, Li S, et al. Choroidal vascularity index assessment: A potential noninvasive technique for diagnosing diabetic nephropathy. *J Ophthalmol*. 2022;2022(1):3124746.
42. Lutty GA, Cao J, McLeod DS. Relationship of polymorphonuclear leukocytes to capillary dropout in the human diabetic choroid. *Am J Pathol*. 1997;151(3):707.
43. Nagaoka T, Kitaya N, Sugawara R, et al. Alteration of choroidal circulation in the foveal region in patients with type 2 diabetes. *Br J Ophthalmol*. 2004;88(8):1060–1063.
44. Muir ER, Rentería RC, Duong TQ. Reduced ocular blood flow as an early indicator of diabetic retinopathy in a mouse model of diabetes. *Invest Ophthalmol Vis Sci*. 2012;53(10):6488–6494.
45. Schocket LS, Brucker AJ, Niknam RM, Grunwald JE, DuPont J, Brucker AJ. Foveolar choroidal hemodynamics in proliferative diabetic retinopathy. *Int Ophthalmol*. 2004;25(2):89–94.
46. Linderman R, Salmon AE, Strampe M, Russillo M, Khan J, Carroll J. Assessing the accuracy of foveal avascular zone measurements using optical coherence tomography angiography: Segmentation and scaling. *Transl Vis Sci Technol*. 2017;6(3):16.
47. Llanas S, Linderman RE, Chen FK, Carroll J. Assessing the use of incorrectly scaled optical coherence tomography angiography images in peer-reviewed studies: A systematic review. *JAMA Ophthalmol*. 2020;138(1):86–94.